



Searching for $0\nu\beta\beta$ with the EXO-200 Experiment -- Results and Prospects

Yale University

Qing (Shilo) Xia

On behalf of the EXO-200 Collaboration

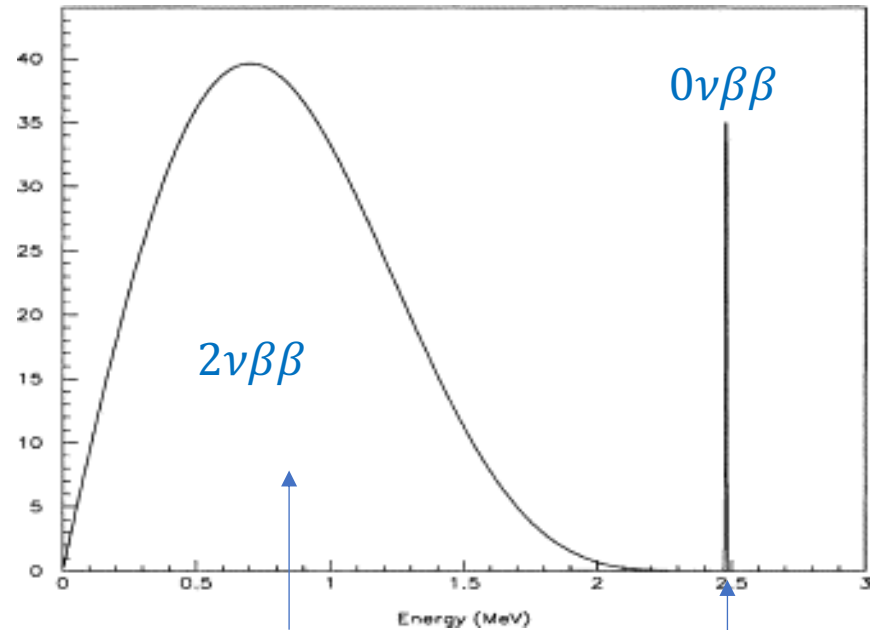
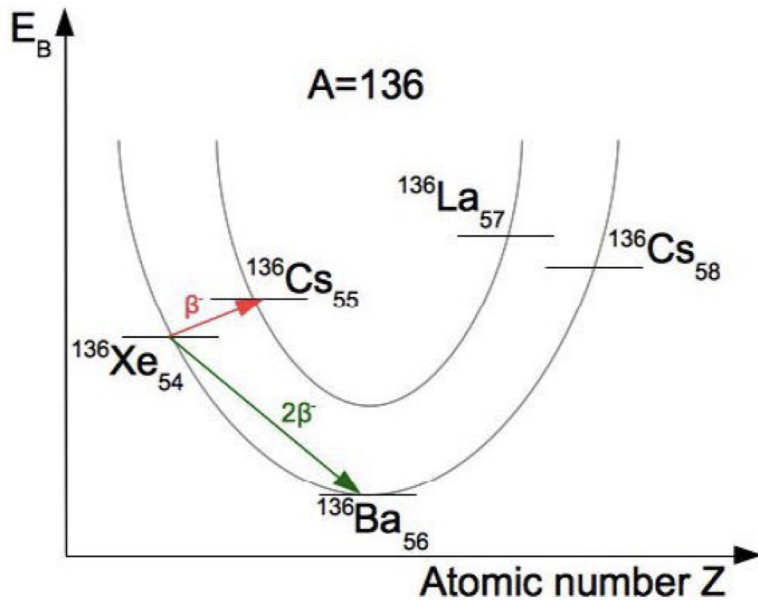
Yale University



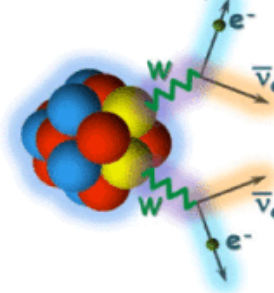
Portal to the Universe

Wright
Laboratory

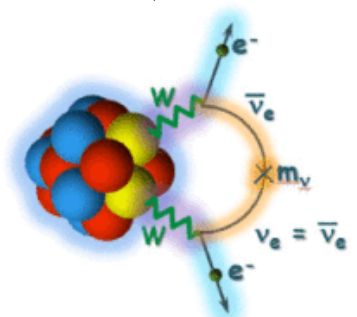
^{136}Xe double beta decay spectrum



[Double beta decay]



Double beta decay which emits anti-neutrinos



Neutrinoless double beta decay

^{136}Xe $2\nu\beta\beta$ decay half life:
 Ref: *Phys. Rev. C* 89, 015502 (2014)

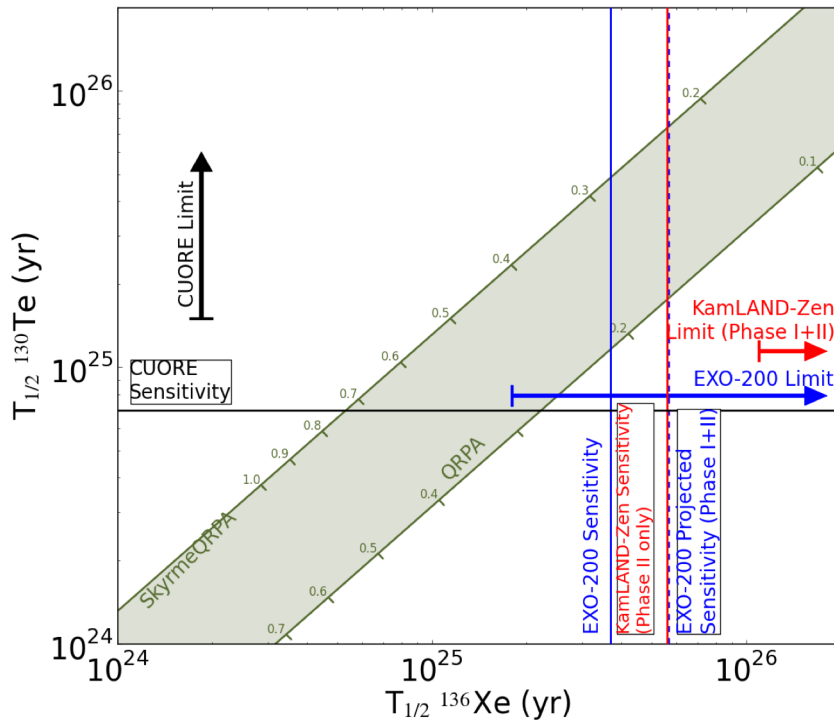
10/20/18 $T_{1/2}(2\nu\beta\beta) = (2.165 \pm 0.016_{stat} \pm 0.059_{sys}) \cdot 10^{21} \text{yr}$

$T_{1/2}(0\nu\beta\beta) \cong ?$

$$0\nu\beta\beta \text{ decay rate } \Gamma = (T_{1/2}^{0\nu})^{-1} = G^{0\nu} |M^{0\nu}|^2 \left| \frac{\langle m_{\beta\beta} \rangle}{m_e} \right|^2$$

- $G^{0\nu}$: phase space factor; $M^{0\nu}$: nuclear matrix element
- $\langle m_{\beta\beta} \rangle = \sum_i U_{ei}^2 m_i$: effective majorana mass

Current limits on $0\nu\beta\beta$ half-life of various isotopes



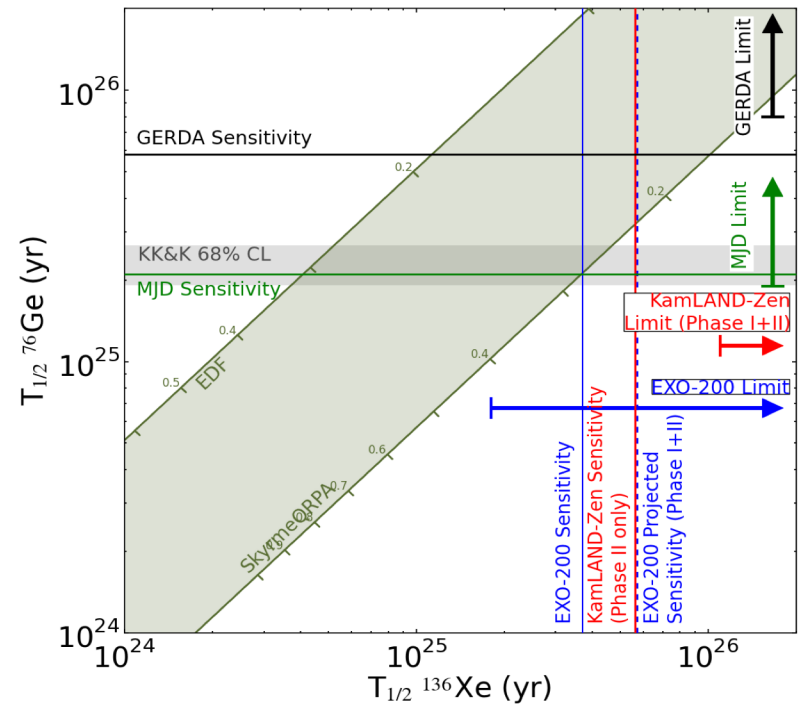
EXO-200: *Phys.Rev.Lett.* 120,072701(2018)

KamLAND-Zen: *PRL* 117 (2016) 082503

CUORE: *Phys. Rev. Lett.* 120, 132501

Skyrme QRPA: *PRC* 87, 064302 (2013)

QRPA: *PRC* 89, 064308 (2014)



EXO-200: *Phys.Rev.Lett.* 120,072701(2018)

GERDA: *Phys. Rev. Lett.* 120, 132503

Majorana: *Phys. Rev. Lett.* 120, 132502

KamLAND-Zen: *PRL* 117 (2016) 082503

KK&K Claim: *Mod. Phys. Lett., A*21 (2006) 1547

EDF: *PRL* 105, 252503 (2010)

University of Alabama, Tuscaloosa AL, USA — M Hughes, O Nusair, I Ostrovskiy, A Piepke, AK Soma, V Veeraraghavan

University of Bern, Switzerland — J-L Vuilleumier

University of California, Irvine, Irvine CA, USA — M Moe

California Institute of Technology, Pasadena CA, USA — P Vogel

Carleton University, Ottawa ON, Canada — I Badhrees, R Gornea, C Jessiman, T Koffas, D Sinclair, B Veenstra, J Watkins

Colorado State University, Fort Collins CO, USA — C Chambers, A Craycraft, D Fairbank, W Fairbank Jr, A Iverson, J Todd

Drexel University, Philadelphia PA, USA — MJ Dolinski, P Gautam, EV Hansen, YH Lin, Y-R Yen

Duke University, Durham NC, USA — PS Barbeau

Friedrich-Alexander-University Erlangen, Nuremberg, Germany — G Anton, J Hoessl, P Hufschmidt, T Michel, M Wagenpfeil, S Schmidt, G Wrede, T Ziegler

IBS Center for Underground Physics, Daejeon, South Korea — DS Leonard

IHEP Beijing, People's Republic of China — G Cao, W Cen, T Tolba, L Wen, J Zhao

ITEP Moscow, Russia — V Belov, A Burenkov, M Danilov, A Dolgolenko, A Karelin, A Kuchenkov, V Stekhanov, O Zeldovich

University of Illinois, Urbana-Champaign IL, USA — D Beck, M Coon, J Echevers, S Li, L Yang

Indiana University, Bloomington IN, USA — JB Albert, SJ Daugherty



Laurentian University, Sudbury ON, Canada — B Cleveland, A Der Mesrobian-Kabakian, J Farine, C Licciardi, A Robinson, U Wichoski

University of Maryland, College Park MD, USA — C Hall

University of Massachusetts, Amherst MA, USA — S Feyzbakhsh, A Pocar, M Tarka

McGill University, Montreal QC, Canada — T Brunner, L Darroch, K Murray

University of North Carolina, Wilmington NC, USA — T Daniels

SLAC National Accelerator Laboratory, Menlo Park CA, USA — M Breidenbach, R Conley, J Davis, S Delaquis, A Johnson, LJ Kaufman,

B Mong, A Odian, CY Prescott, PC Rowson, JJ Russell, K Skarpaas, A Waite, M Wittgen

University of South Dakota, Vermillion SD, USA — A Larson, R MacLellan

Stanford University, Stanford CA, USA — J Dalmasson, R DeVoe, D Fudenberg, G Gratta, M Jewell, S Kravitz, G Li, A Schubert, M Weber, S Wu

Stony Brook University, SUNY, Stony Brook, NY, USA — K Kumar, O Njoya

Technical University of Munich, Garching, Germany — W Feldmeier, P Fierlinger, M Marino

TRIUMF, Vancouver BC, Canada — J Dilling, R Krücken, Y Lan, F Retière, V Strickland

Yale University, New Haven CT, USA — A Jamil, Z Li, D Moore, Q Xia

EXO-200 at WIPP



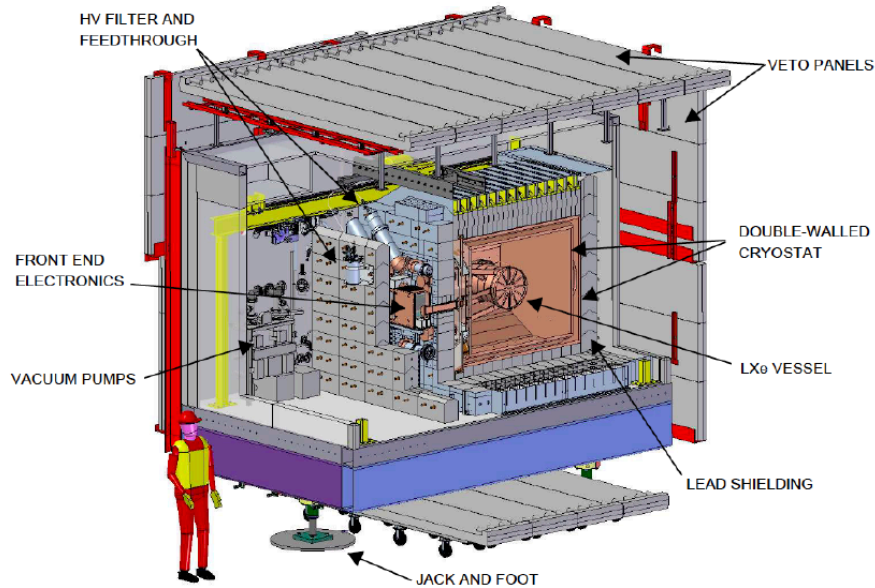
Carlsbad, NM
WIPP/EXO

Bat Flight

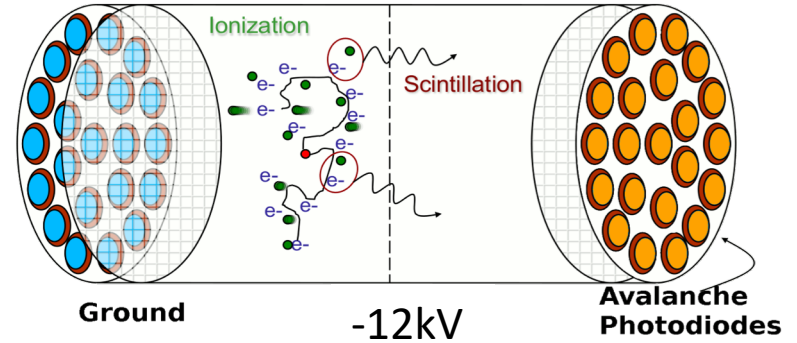
Carlsbad Caverns

10/20/18

Design of the EXO-200 detector



Charge and light energy deposit in the TPC



TPC design

crossed charge wires (photo-etched phosphor bronze)

10/20/18

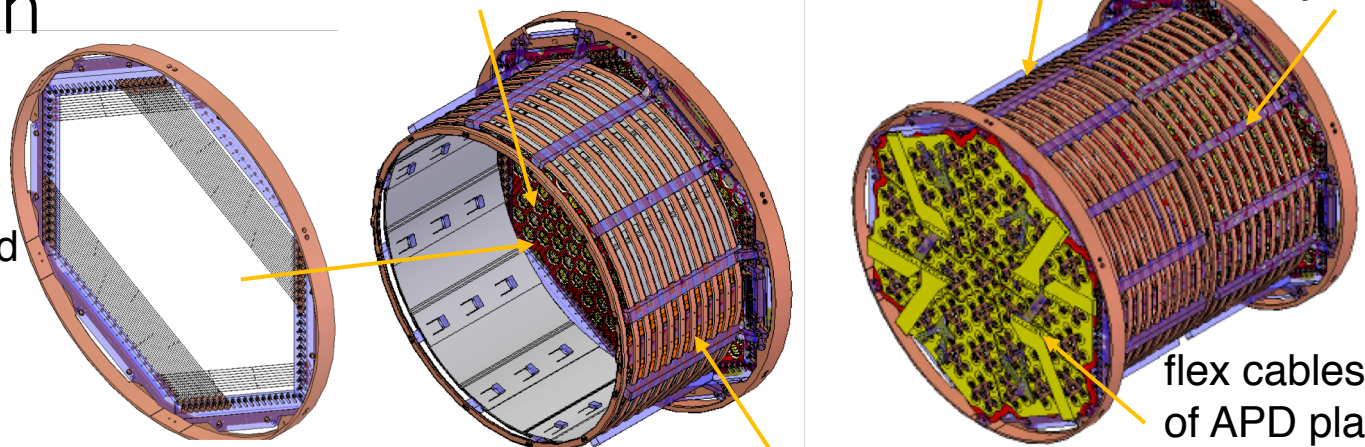
APD plane

Central HV plane

acrylic supports

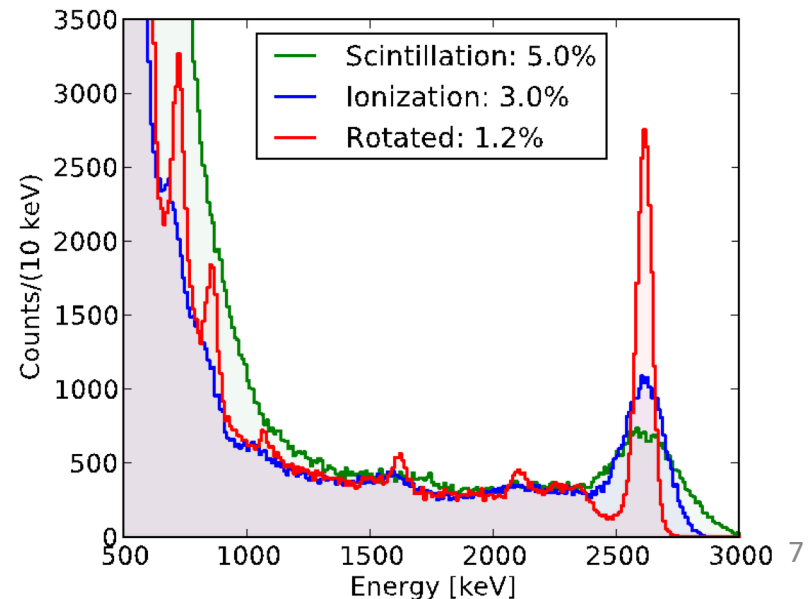
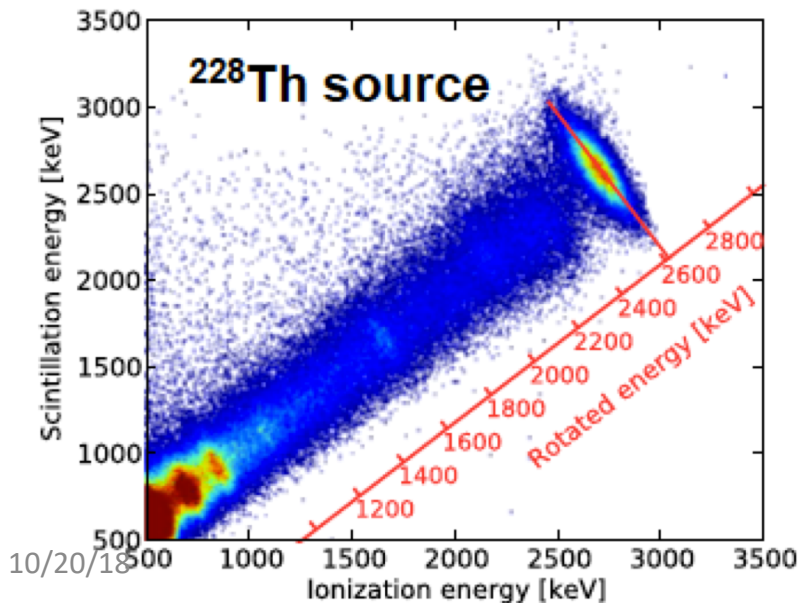
field shaping rings (copper)

flex cables on back of APD plane (copper on kapton)

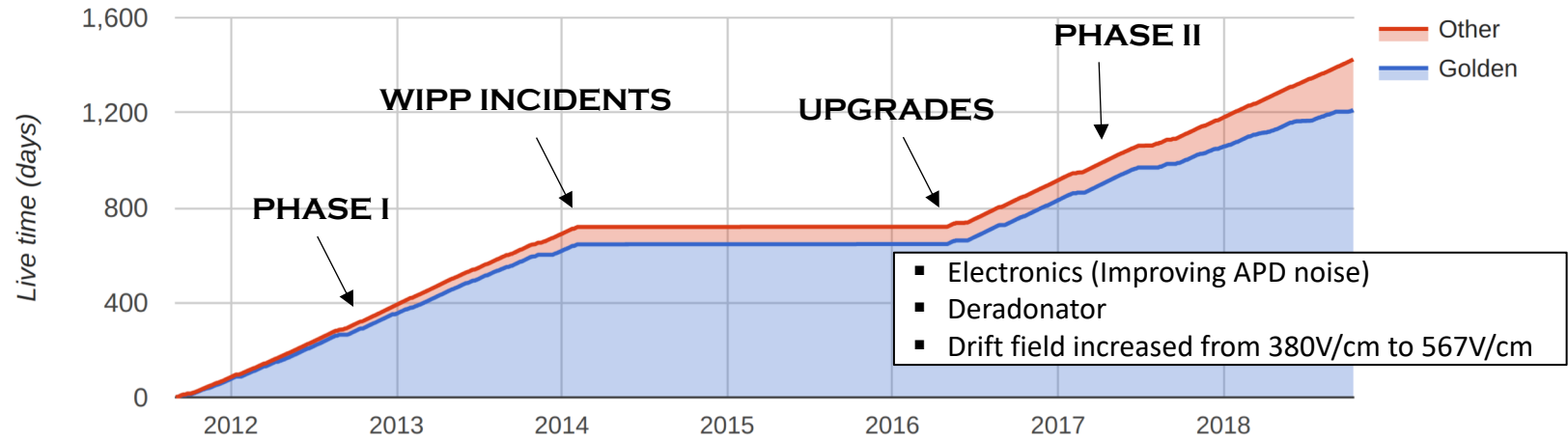


Energy resolution of the detector

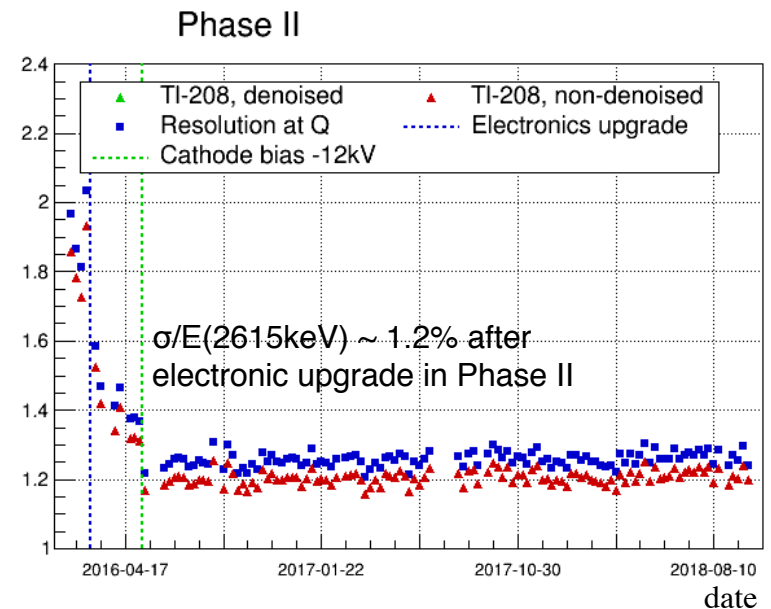
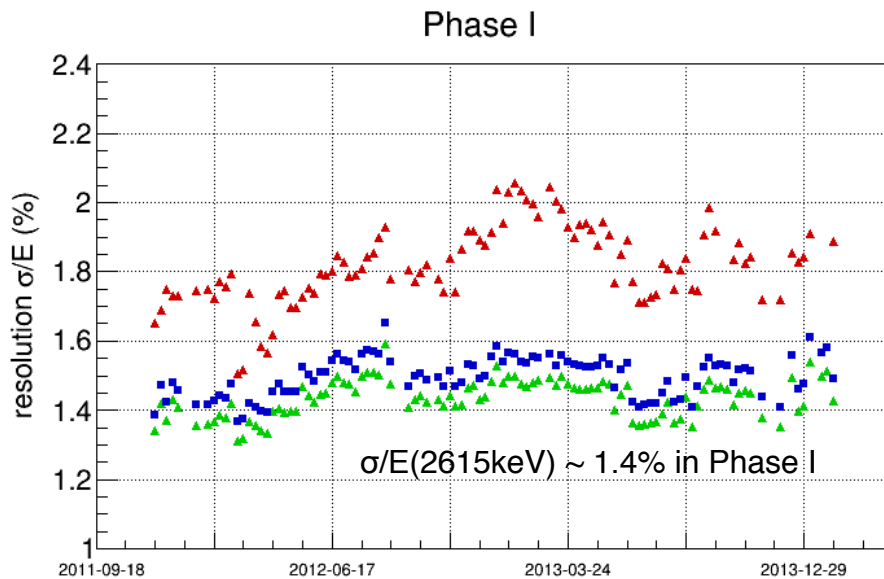
- An incident particle generates both charge and light signals the detector
- The elliptical island in the 2D energy histogram below demonstrates the anti-correlation between charge and light energy deposition
- To optimize the energy resolution, we introduce a rotated energy $E_r = E_s \sin \theta + E_c \cos \theta$ (E_s is scintillation energy, E_c is ionization energy)



EXO-200 operation



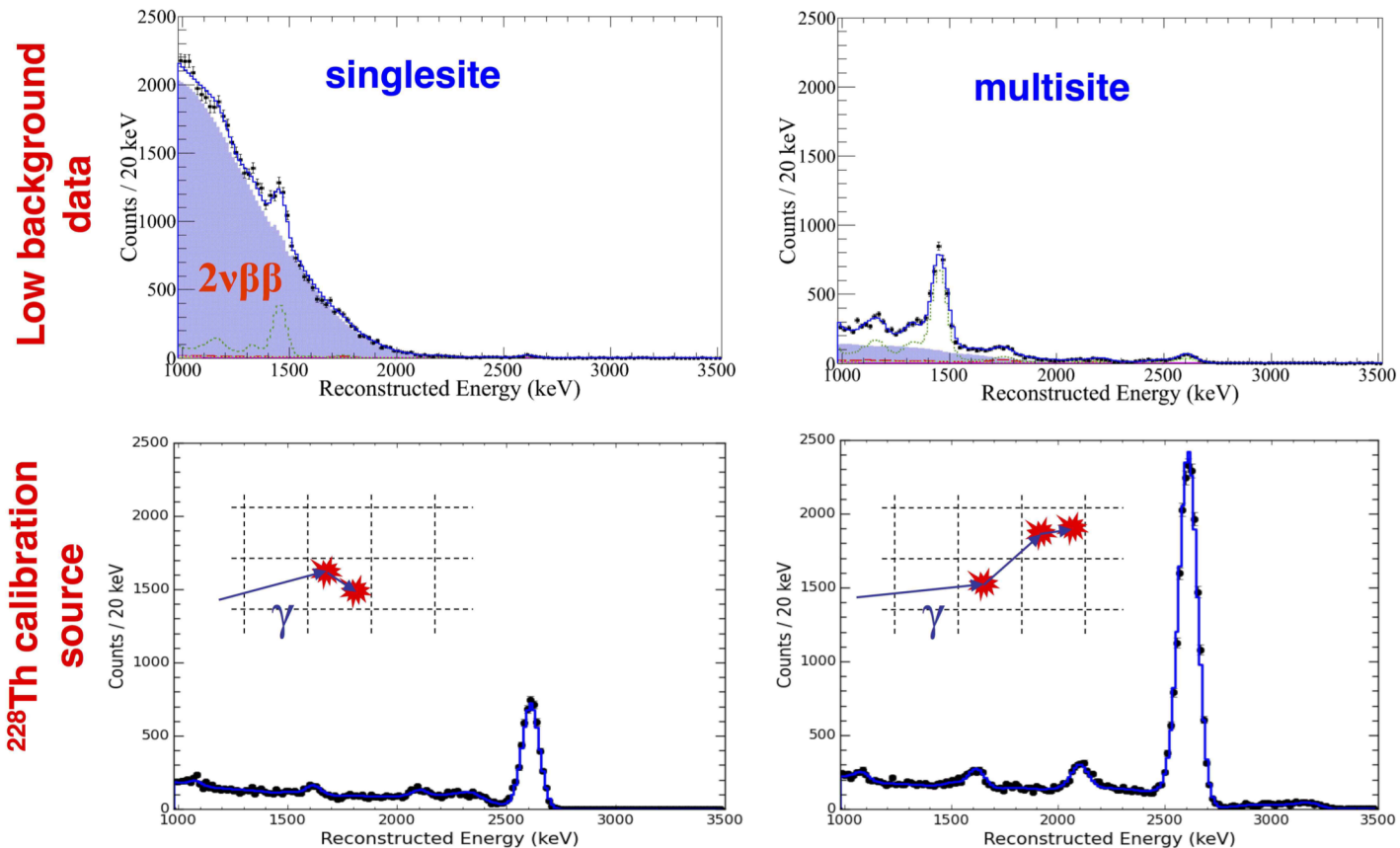
Energy resolution vs. time



10/20/18 • Energy resolution is improved from 1.4% to 1.2% after electronic upgrade

EXO-200 signal/background discrimination

- Topological classification provides good signal/background discrimination
- Electron-like signal events (e.g. $2\nu\beta\beta$) are predominantly single-sited, while gamma-like background events are mostly multi-sited

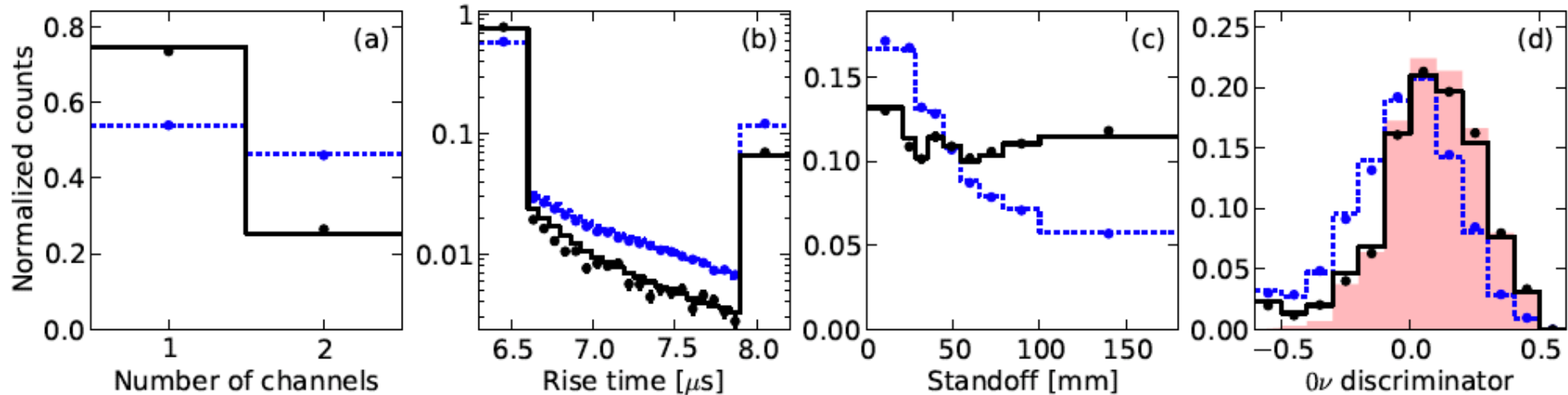
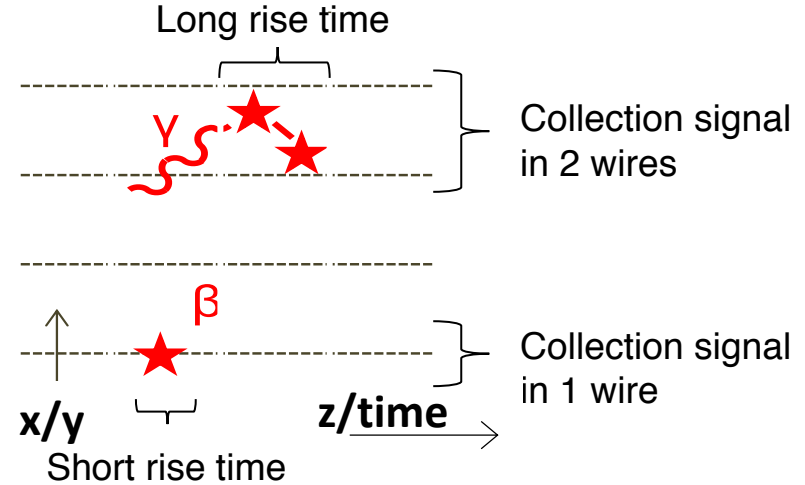


Improved analysis for Phase II

Multi-variate discriminator improves signal/background separation:

- Number of channels hit by the charge cluster
- Rise time of the charge pulse
- Standoff distance

Improved sensitivity by $\sim 15\%$

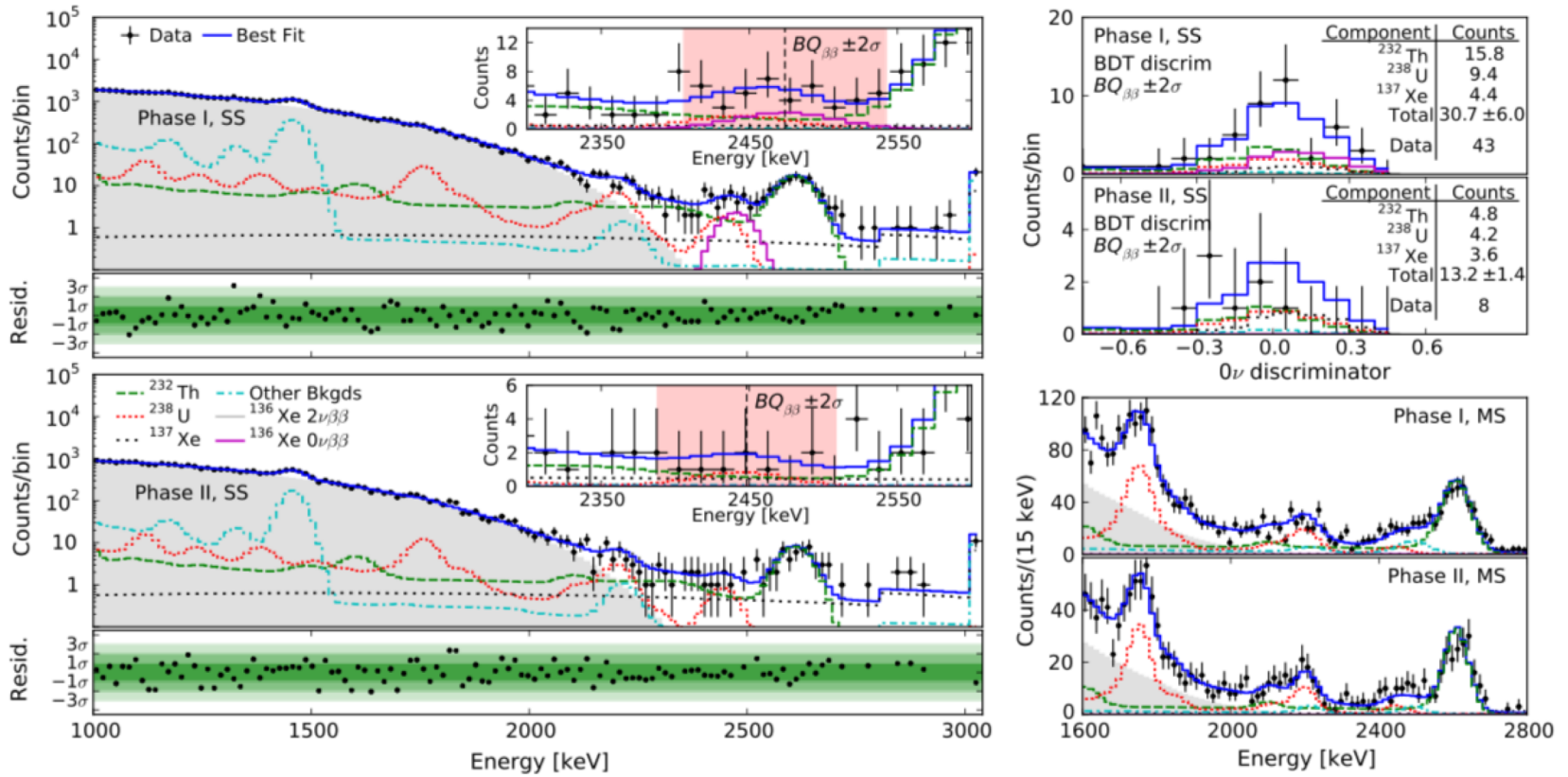


Black dots — $2\nu\beta\beta$ data; Black lines — $2\nu\beta\beta$ MC;
 Blue dots — ^{226}Ra data; Blue lines — ^{226}Ra MC.

Phys. Rev. Lett. 120, 072701 (2018)

Red region — MC of the expected BDT discriminator distribution for a $0\nu\beta\beta$ signal

Comparison between energy spectrum for Phase I and Phase II

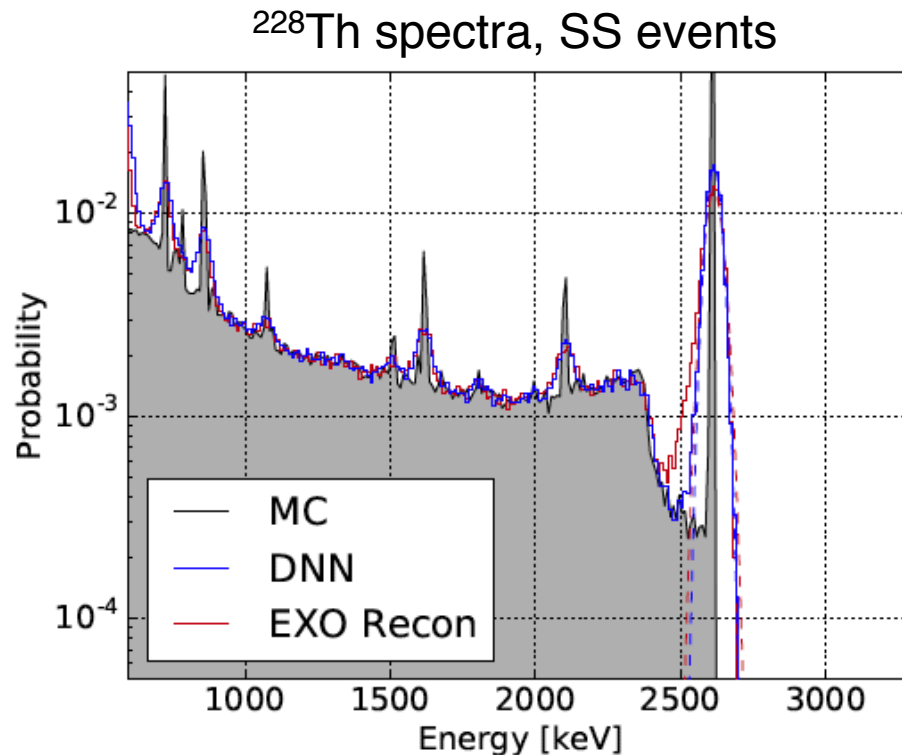


EXO-200	Sensitivity	Limit, 90%CL
2012	0.7×10^{25} yr	1.6×10^{25} yr
2014	1.9×10^{25} yr	1.1×10^{25} yr
2018	3.7×10^{25} yr	1.8×10^{25} yr

Phys. Rev. Lett. 120, 072701 (2018)

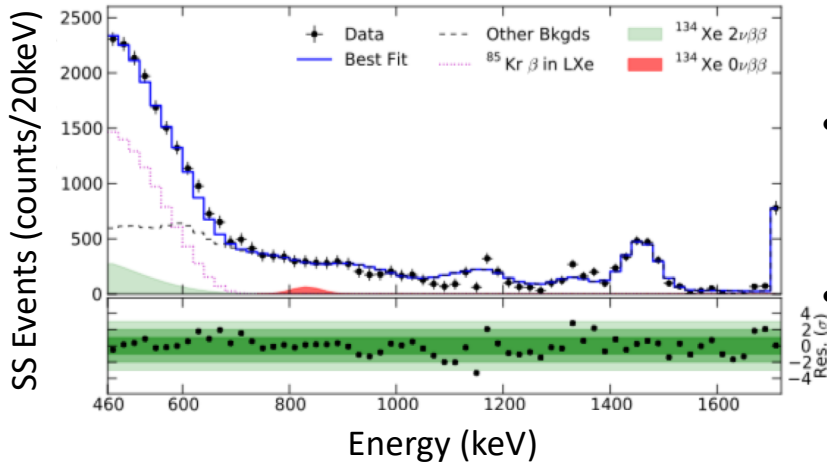
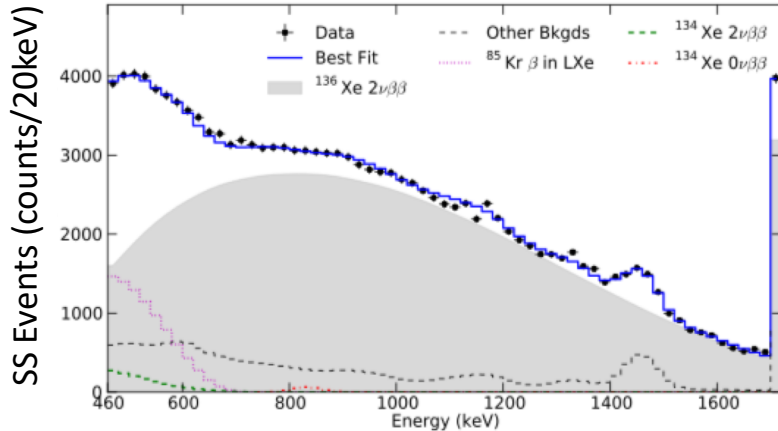
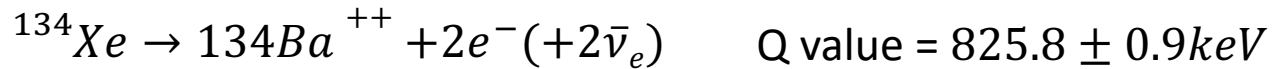
Deep Neural Networks (DNN) for Charge Energy Reconstruction

- Monte Carlo simulation generates a large number of events for which the “true charge energy” is known.
- DNN extracts energy directly from 76 charge readout channels’ waveform patterns.
- DNN reconstructs a better charge energy resolution than the standard EXO reconstruction method.



2018 JINST 13 P08023

Search for double beta decay of ^{134}Xe



- Results from EXO-200 measurement (*Phys. Rev. D* 96, 092001, 2017):

$$T_{1/2}^{2\nu\beta\beta} > 8.7 \times 10^{20} \text{ yr at 90\% C.L.}$$

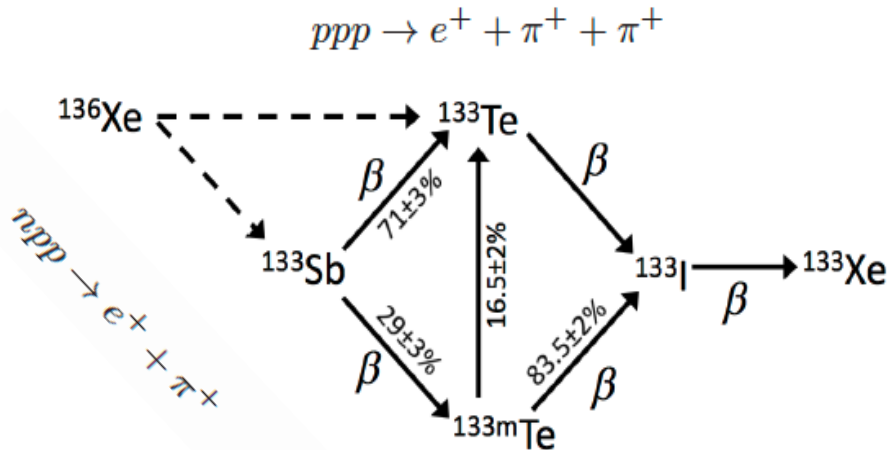
(Theoretical value: $\sim 10^{24} - 10^{25} \text{ yr}$)

$$T_{1/2}^{0\nu\beta\beta} > 1.1 \times 10^{23} \text{ yr at 90\% C.L.}$$

- Improved by factors of 10^5 and 2 respectively compared to previous measurements.
- Lower scintillation noise and reduced ^{85}Kr in Phase II will improve search sensitivity

Search for nucleon decay using EXO-200

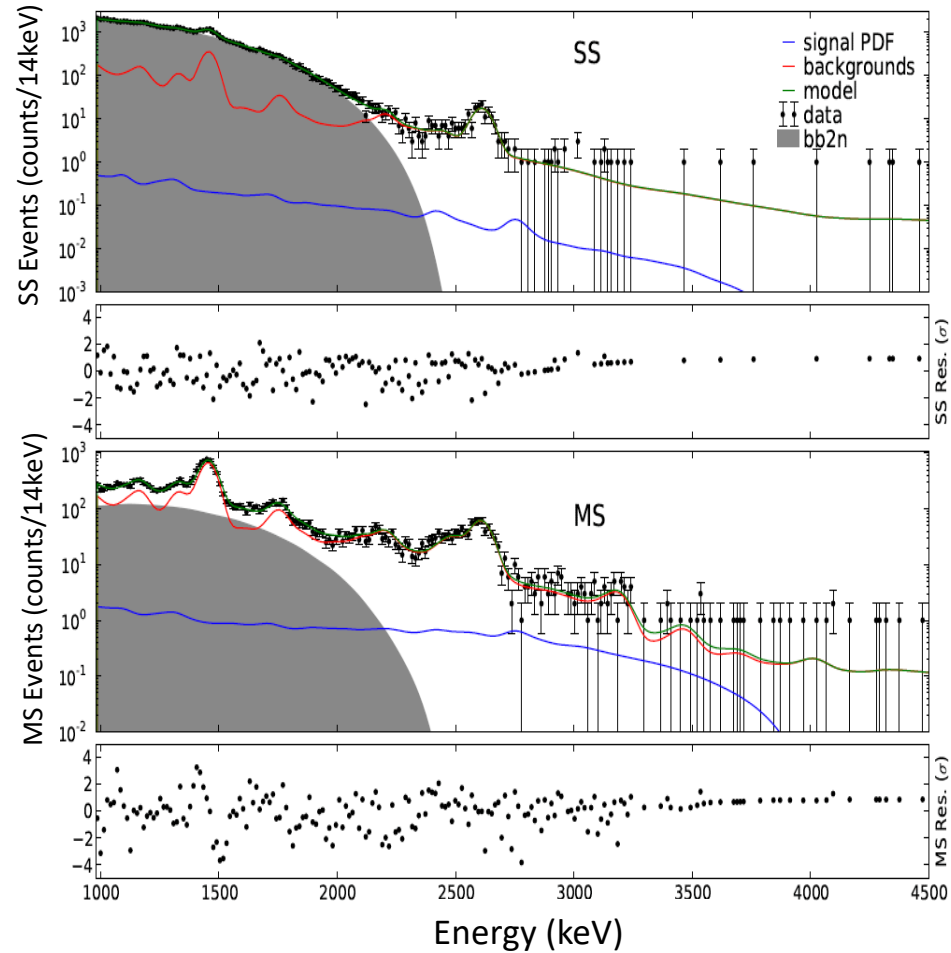
- Searched for exotic nucleon decay with $\Delta B = 3$
- Tested at $\Lambda \sim 10^2$ GeV energy scale



- Lifetime limits for ^{133}Sb : 3.3×10^{23} yr
- Lifetime limits for ^{133}Te : 1.9×10^{23} yr
- Exceeding the prior decay limits by a factor of 9 and 7, respectively

10/20/18

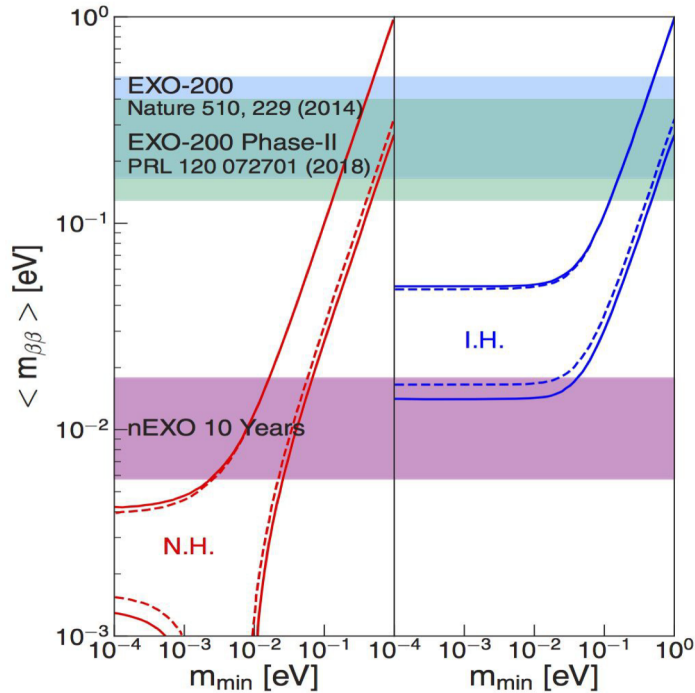
Best-fit model for decay to ^{133}Sb :



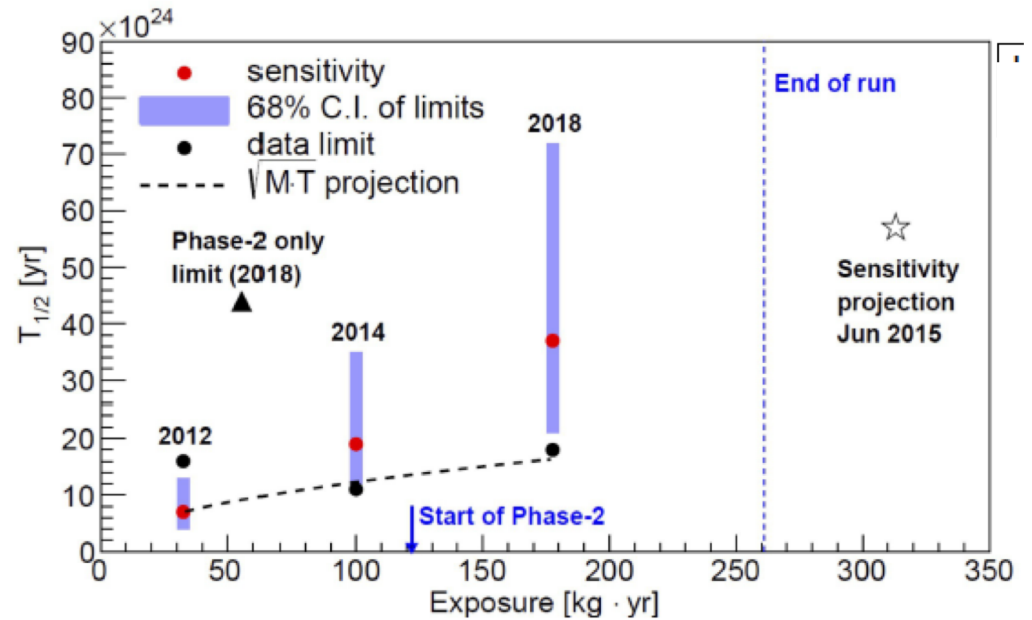
Phys. Rev. D 97, 072007 (2018)

Conclusion

- EXO-200 demonstrated the potential of monolithic / homogenous LXe detectors
- Detector sensitivity improved by a factor two ($1.9 \cdot 10^{25}$ yr in 2014, $3.7 \cdot 10^{25}$ yr in 2018)



EXO-200 detector sensitivity



- $T_{1/2}^{0\nu\beta\beta}({}^{136}\text{Xe}) > 1.8 \times 10^{25}$ yr, $\langle m_{\beta\beta} \rangle < (147 - 398) \text{ meV}$
- Significant improvement in the measurement of triple nucleon decay half-life
- Final results will follow after the end of Phase II at the end of year
- R&D towards a tonne-scale detector nEXO on the way, will reach a sensitivity of 10^{28} yr

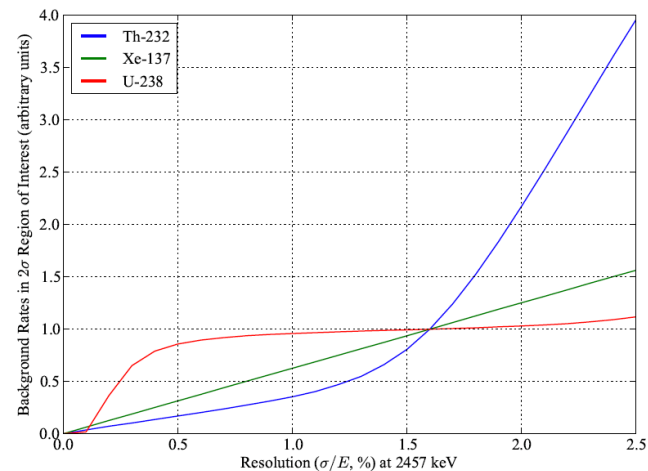
Mahalo for your attention!

Backup slides

Experimental backgrounds and the importance of the detector's resolution

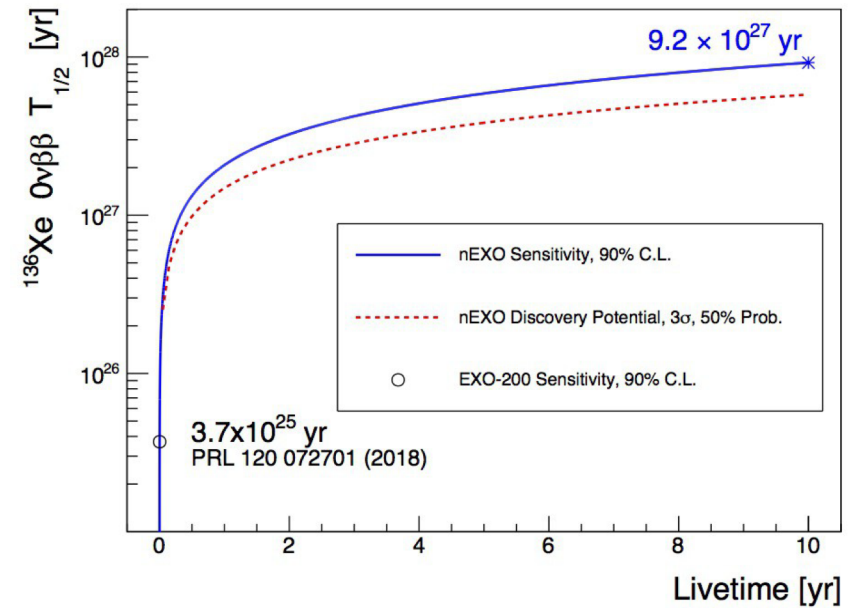
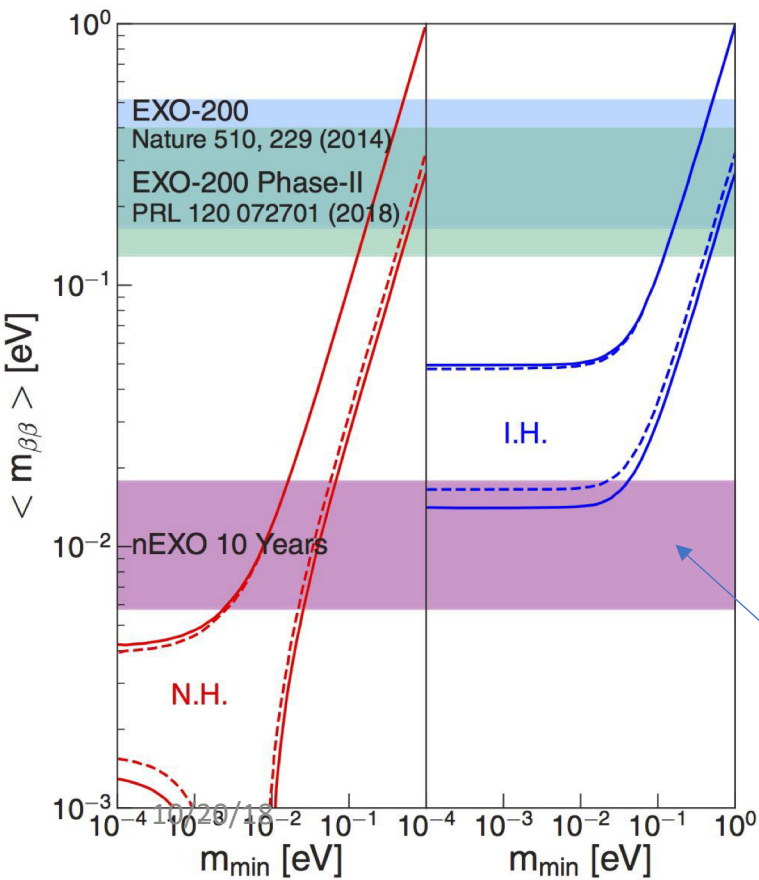
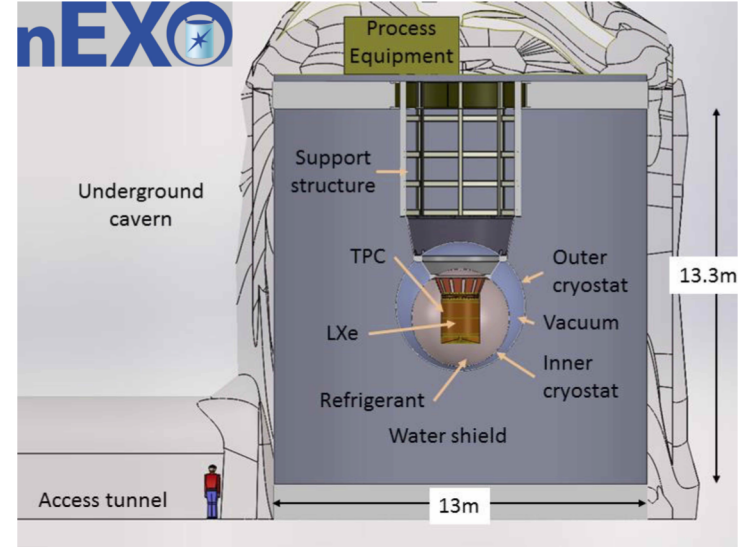
- Signal: $^{136}\text{Xe } 0\nu\beta\beta$'s signature mono-energetic peak at $Q=2458$ keV
- Main backgrounds :
 - $^{137}\text{Xe } \beta$ decay with an endpoint energy of 4173 keV.
 - ^{208}Tl from ^{232}Th decay chain--gamma peak 2615 keV; Compton edge at 2382 keV.
 - ^{214}Bi from ^{238}U decay chain-- gamma at 2448 keV

Relative change in background rates expected in our 2σ region of interest as a function of the energy resolution:



- The energy resolution near the region of Q value is of utmost importance for the sensitivity of the experiment.

nEXO – the next generation tonne-scale LXe detector

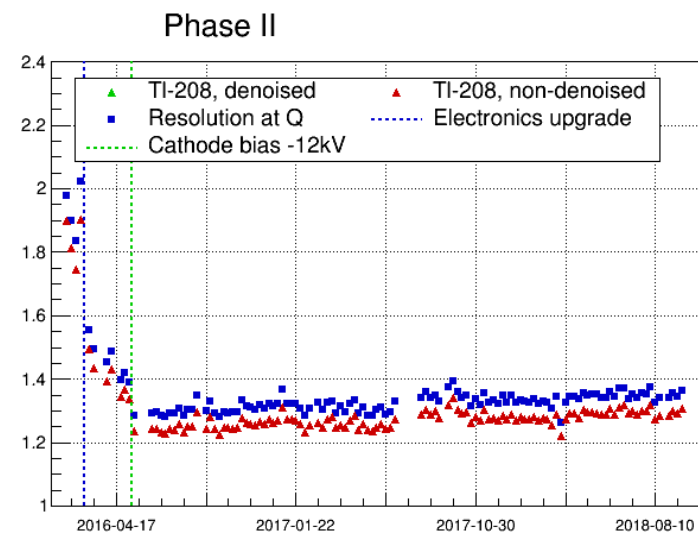
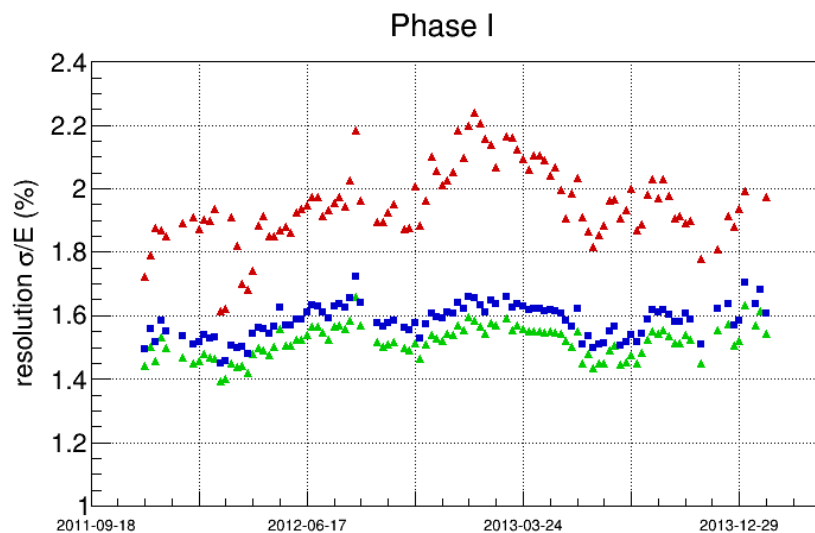


- Width of the bands represent the uncertainties in nuclear matrix elements
- Assumes axial vector constant $g_A = 1.27$

Advantages of LXe TPCs

- Xenon isotopic enrichment is relatively safe and easy
- Can be recycled and purified in to new detectors
- No long lived radioactive isotopes of Xe
- Background can be significantly reduced through daughter Ba tagging
- Fair energy resolution

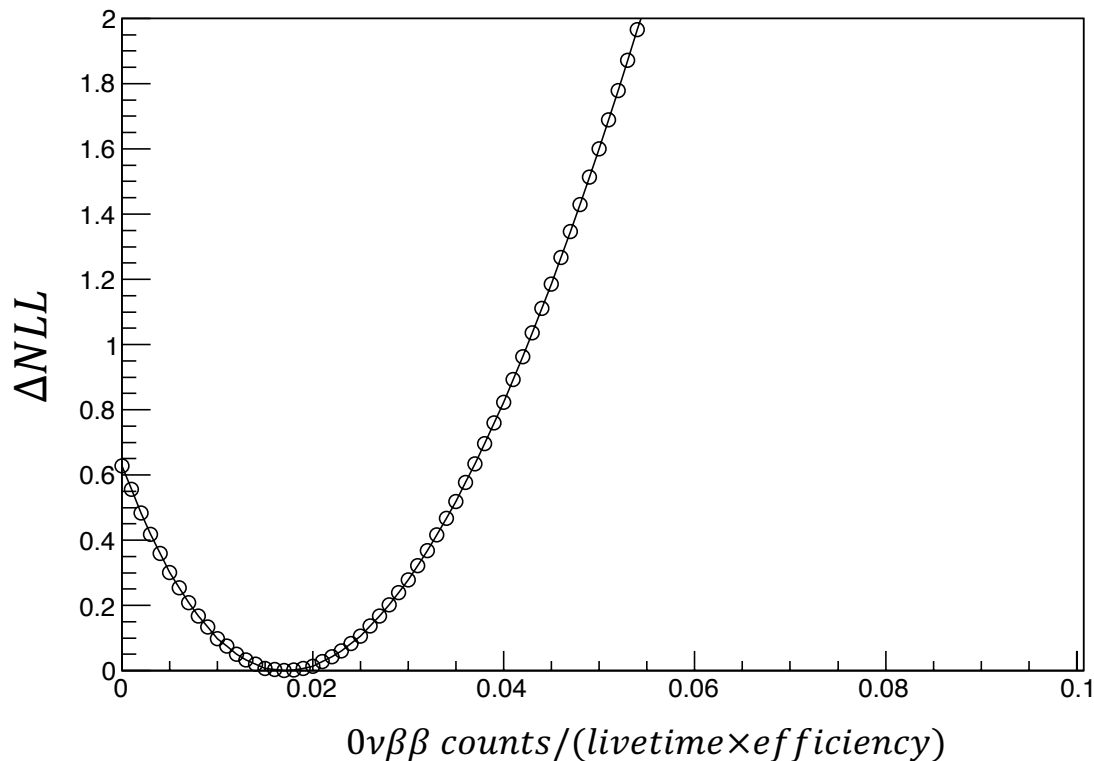
Resolution vs. time (multi-site events)



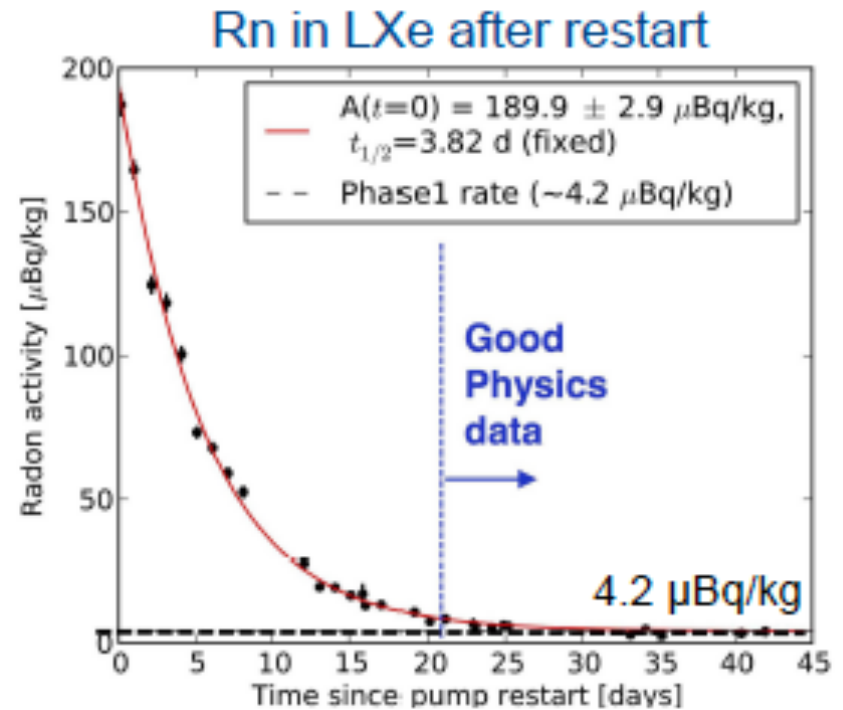
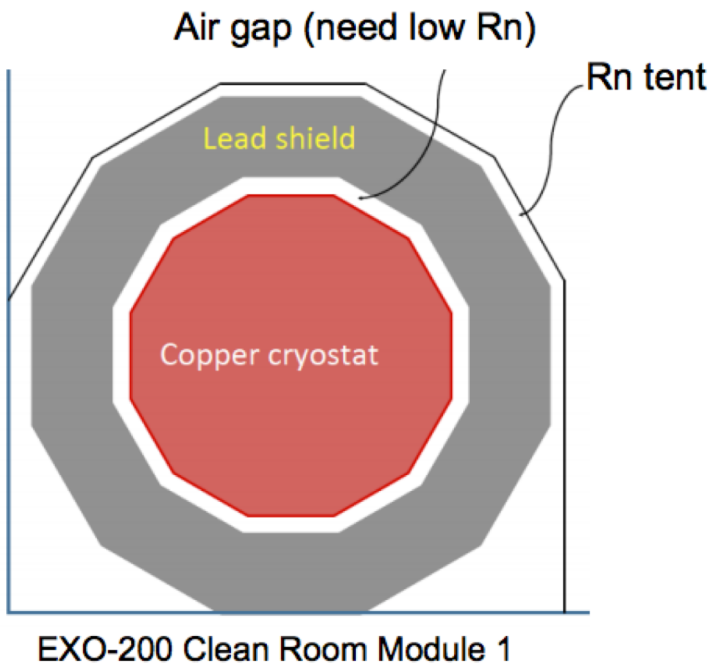
Phase I + Phase II likelihood profile

- The negative log likelihood function used in profile-likelihood

$$-\ln L = \sum_i [(\mu_i^{\text{SS}} + \mu_i^{\text{MS}}) - (k_{\text{obs},i}^{\text{SS}} \ln \mu_i^{\text{SS}} + k_{\text{obs},i}^{\text{MS}} \ln \mu_i^{\text{MS}})] + G_{\text{const}}$$



Radon activity



Uncertainties on nuclear matrix elements

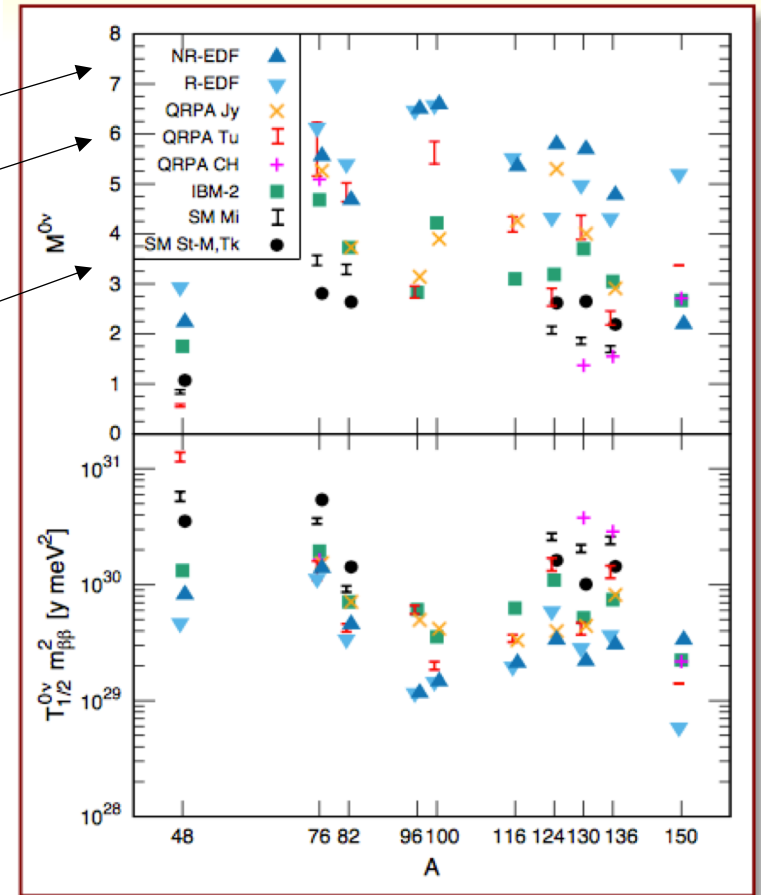
Minimizing an energy functional with respect to local densities (but no n-p pairing)

QRPA involves small oscillations around a single determinant and quasi-particle states

Slater determinants restricted to a few single-particle shells

Decay Rate

$$\Gamma = \left(T_{\frac{1}{2}}^{0\nu}\right)^{-1} = \underbrace{G^{0\nu}}_{\text{Phase space}} \underbrace{|M^{0\nu}|^2}_{\text{Nuclear Matrix Element}} \underbrace{\left|\frac{\langle m_{\beta\beta} \rangle}{m_e}\right|^2}_{\text{Effective Majorana Mass}}$$



J.Engel and J. Menendez
arXiv:1610.06548v2

NMEs

For phase space I take the values of Kotila and Iachello (PRC85,034316)
24.81x10⁻¹⁵ for Ca48, 2.363x10⁻¹⁵ (Ge), 14.22x10⁻¹⁵ (Te) and 14.58x10⁻¹⁵ for Xe136.

To convert it into the formula $1/T_{1/2} = G^{0\nu} |M|^2 \langle m_{\nu\nu} \rangle^2$ where $\langle m_{\nu\nu} \rangle$ is in eV
one needs to divide this by m_e^2 and multiply by g_A^4 . This gives $(G^{0\nu})^{-1} = 4.05 \times 10^{24}$
(Ca), 4.24x10²⁵ (Ge), 7.056x10²⁴(Te) and 6.88x10²⁴(Xe).

For matrix elements I take the following sources:

IBM, Barnea, Kotila, Iachello, PRC87, 014315: 2.33 (Ca), 6.07(Ge), 4.54(Te), 3.73(Xe)

EDF, Rodriguez, Martinez-Pinedo, PRL105, 252503: 2.37(Ca), 4.60(Ge),
5.13(Te),4.20(Xe)

QRPA, Engel, Simkovic, Vogel, PRC89, 064308 : 0.61(Ca), 4.64(Ge), 3.65(Te),2.02(Xe)

NSM, Menendez et al., NPA818, 139: 0.85(Ca), 2.81(Ge), 2.65(Te), 2.19(Xe)

$$\langle m_{\nu\nu} \rangle = 1/M_{Xe} \times 1/(G_{Xe})^{1/2} \times 1/(T_{1/2}^{Xe})^{1/2}$$

where $1/G_{Xe}$ and $T_{1/2}$ are in 10²⁴ units and $\langle m_{\nu\nu} \rangle$ is in eV

Thus $\langle m_{\nu\nu} \rangle$ (eV)x(T_{1/2}^{Xe})^{1/2} = 0.703(IBM), 0.625(EDF), 1.29 (QRPA), 1.20(NSM)